The Astrophysical Journal, 706:L138–L144, 2009 November 20 doi:10.1088/0004-637X/706/1/L138

FERMI OBSERVATIONS OF GRB 090902B: A DISTINCT SPECTRAL COMPONENT IN THE PROMPT AND DELAYED EMISSION

A. A. Abdo[1,2], M. Ackermann[3], M. Ajello[3], K. Asano[4,5], W. B. Atwood[6], M. Axelsson[7,8], L. Baldini[9], J. Ballet[10], G. Barbiellini[11,12], M. G. Baring[13], D. Bastieri[14,15], K. Bechtol[3], R. Bellazzini[9], B. Berenji[3], P. N. Bhat[16], E. Bissaldi[17], R. D. Blandford[3], E. D. Bloom[3], E. Bonamente[18,19], A. W. Borgland[3], A. Bouvier[3], J. Bregeon[9], A. Brez[9], M. S. Briggs[16], M. Brigida[20,21], P. Bruel[22], J. M. Burgess[16], D. N. Burrows[23], S. Buson[15], G. A. Caliandro[20,21], R. A. Cameron[3], P. A. Caraveo[24], J. M. Casandjian[10], C. Cecchi[18,19], Ö. Çelik[25,26,27], A. Chekhtman[1,28], C. C. Cheung[1,2,25], J. Chiang[3], S. Ciprini[18,19], R. Claus[3], J. Cohen-Tanugi[29], L. R. Cominsky[30], V. Connaughton[16], J. Conrad[8,31,63], S. Cutini[32], V. d'Elia[32], C. D. Dermer[1], A. de Angelis[33], F. de Palma[20,21], S. W. Digel[3], B. L. Dingus[34], E. do Couto e Silva[3], P. S. Drell[3], R. Dubois[3], D. Dumora[35,36], C. Farnier[29], C. Favuzzi[20,21], S. J. Fegan[22], J. Finke[1,2], G. Fishman[37], W. B. Focke[3], P. Fortin[22], M. Frailis[33], Y. Fukazawa[38], S. Funk[3], P. Fusco[20,21], F. Gargano[21], N. Gehrels[23,25,39], S. Germani[18,19], G. Giavitto[40], B. Giebels[22], N. Giglietto[20,21], F. Giordano[20,21], T. Glanzman[3], G. Godfrey[3], A. Goldstein[16], J. Granot[41], J. Greiner[17], I. A. Grenier[10], J. E. Grove[1], L. Guillemot[42], S. Guiriec[16], Y. Hanabata[38], A. K. Harding[25], M. Hayashida[3], E. Hays[25], D. Horan[22], R. E. Hughes[43], M. S. Jackson[8,31,44], G. Jóhannesson[3], A. S. Johnson[3], R. P. Johnson[6], W. N. Johnson[1], T. Kamae[3], H. Katagiri[38], J. Kataoka[4,45], N. Kawai[4,46], M. Kerr[47], R. M. Kippen[34], J. Knödlseder[48], D. Kocevski[3], N. Komin[10,29], C. Kouveliotou[37], M. Kuss[9], J. Lande[3], L. Latronico[9], M. Lemoine-Goumard[35,36], F. Longo[11,12], F. Loparco[20,21], B. Lott[35,36], M. N. Lovellette[1], P. Lubrano[18,19], G. M. Madejski[3], A. Makeev[1,28], M. N. Mazziotta[21], S. McBreen[17,49], J. E. McEnery[25,39], S. McGlynn[8,44], C. Meegan[50], P. Mészáros[23], C. Meurer[8,31], P. F. Michelson[3], W. Mitthumsiri[3], T. Mizuno[38], A. A. Moiseev[26,39], C. Monte[20,21], M. E. Monzani[3], E. Moretti[11,12,40], A. Morselli[51], I. V. Moskalenko[3], S. Murgia[3], T. Nakamori[4], P. L. Nolan[3], J. P. Norris[52], E. Nuss[29], M. Ohno[53], T. Ohsugi[38], N. Omodei[9], E. Orlando[17], J. F. Ormes[52], W. S. Paciesas[16], D. Paneque[3], J. H. Panetta[3], V. Pelassa[29], M. Pepe[18,19], M. Pesce-Rollins[9], V. Petrosian[3], F. Piron[29], T. A. Porter[6], R. Preece[16], S. Rainò[20,21], R. Rando[14,15], A. Rau[17], M. Razzano[9], S. Razzaque[1,2], A. Reimer[3,54], O. Reimer[3,54], T. Reposeur[35,36], S. Ritz[6], L. S. Rochester[3], A. Y. Rodriguez[55], P. W. A. Roming[23], M. Roth[47], F. Ryde[8,44], H. F.-W. Sadrozinski[6], D. Sanchez[22], A. Sander[43], P. M. Saz Parkinson[6], J. D. Scargle[56], T. L. Schalk[6], C. Sgrò[9], E. J. Siskind[57], P. D. Smith[43], P. Spinelli[20,21], M. Stamatikos[25,43], F. W. Stecker[25], G. Stratta[32], M. S. Strickman[1], D. J. Suson[58], C. A. Swenson[23], H. Tajima[3], H. Takahashi[38], T. Tanaka[3], J. B. Thayer[3], J. G. Thayer[3], D. J. Thompson[25], L. Tibaldo[10,14,15], D. F. Torres[55,59], G. Tosti[18,19], A. Tramacere[3,60], Y. Uchiyama[3,53], T. Uehara[38], T. L. Usher[3], A. J. van der Horst[37,64], V. Vasileiou[25,26,27], N. Vilchez[48], V. Vitale[51,61], A. von Kienlin[17], A. P. Waite[3], P. Wang[3], C. Wilson-Hodge[37], B. L. Winer[43], K. S. Wood[1], R. Yamazaki[38], T. Ylinen[8,44,62], and M. Ziegler[6]

[1] Space Science Division, Naval Research Laboratory, Washington, DC 20375, USA
[2] National Research Council Research Associate, National Academy of Sciences, Washington, DC 20001, USA
[3] W. W. Hansen Experimental Physics Laboratory, Kavli Institute for Particle Astrophysics and Cosmology, Department of Physics and SLAC National Accelerator Laboratory, Stanford University, Stanford, CA 94305, USA
[4] Department of Physics, Tokyo Institute of Technology, Meguro City, Tokyo 152-8551, Japan
[5] Interactive Research Center of Science, Tokyo Institute of Technology, Meguro City, Tokyo 152-8551, Japan
[6] Santa Cruz Institute for Particle Physics, Department of Physics and Department of Astronomy and Astrophysics, University of California at Santa Cruz, Santa Cruz, CA 95064, USA
[7] Department of Astronomy, Stockholm University, SE-106 91 Stockholm, Sweden
[8] The Oskar Klein Centre for Cosmoparticle Physics, AlbaNova, SE-106 91 Stockholm, Sweden
[9] Istituto Nazionale di Fisica Nucleare, Sezione di Pisa, I-56127 Pisa, Italy
[10] Laboratoire AIM, CEA-IRFU/CNRS/Université Paris Diderot, Service d'Astrophysique, CEA Saclay, 91191 Gif sur Yvette, France
[11] Istituto Nazionale di Fisica Nucleare, Sezione di Trieste, I-34127 Trieste, Italy
[12] Dipartimento di Fisica, Università di Trieste, I-34127 Trieste, Italy
[13] Rice University, Department of Physics and Astronomy, MS-108, P.O. Box 1892, Houston, TX 77251, USA
[14] Istituto Nazionale di Fisica Nucleare, Sezione di Padova, I-35131 Padova, Italy
[15] Dipartimento di Fisica "G. Galilei," Università di Padova, I-35131 Padova, Italy
[16] University of Alabama in Huntsville, Huntsville, AL 35899, USA
[17] Max-Planck Institut für extraterrestrische Physik, 85748 Garching, Germany
[18] Istituto Nazionale di Fisica Nucleare, Sezione di Perugia, I-06123 Perugia, Italy
[19] Dipartimento di Fisica, Università degli Studi di Perugia, I-06123 Perugia, Italy
[20] Dipartimento di Fisica "M. Merlin" dell'Università e del Politecnico di Bari, I-70126 Bari, Italy
[21] Istituto Nazionale di Fisica Nucleare, Sezione di Bari, 70126 Bari, Italy
[22] Laboratoire Leprince-Ringuet, École polytechnique, CNRS/IN2P3, Palaiseau, France
[23] Department of Astronomy and Astrophysics, Pennsylvania State University, University Park, PA 16802, USA
[24] INAF-Istituto di Astrofisica Spaziale e Fisica Cosmica, I-20133 Milano, Italy
[25] NASA Goddard Space Flight Center, Greenbelt, MD 20771, USA
[26] Center for Research and Exploration in Space Science and Technology (CRESST), NASA Goddard Space Flight Center, Greenbelt, MD 20771, USA
[27] University of Maryland, Baltimore County, Baltimore, MD 21250, USA
[28] George Mason University, Fairfax, VA 22030, USA
[29] Laboratoire de Physique Théorique et Astroparticules, Université Montpellier 2, CNRS/IN2P3, Montpellier, France
[30] Department of Physics and Astronomy, Sonoma State University, Rohnert Park, CA 94928-3609, USA
[31] Department of Physics, Stockholm University, AlbaNova, SE-106 91 Stockholm, Sweden
[32] Agenzia Spaziale Italiana (ASI) Science Data Center, I-00044 Frascati (Roma), Italy

[33] Dipartimento di Fisica, Università di Udine and Istituto Nazionale di Fisica Nucleare, Sezione di Trieste, Gruppo Collegato di Udine, I-33100 Udine, Italy
[34] Los Alamos National Laboratory, Los Alamos, NM 87545, USA
[35] Université de Bordeaux, Centre d'Études Nucléaires Bordeaux Gradignan, UMR 5797, Gradignan, 33175, France
[36] CNRS/IN2P3, Centre d'Études Nucléaires Bordeaux Gradignan, UMR 5797, Gradignan, 33175, France
[37] NASA Marshall Space Flight Center, Huntsville, AL 35812, USA
[38] Department of Physical Sciences, Hiroshima University, Higashi-Hiroshima, Hiroshima 739-8526, Japan
[39] University of Maryland, College Park, MD 20742, USA
[40] Istituto Nazionale di Fisica Nucleare, Sezione di Trieste, and Università di Trieste, I-34127 Trieste, Italy
[41] Centre for Astrophysics Research, University of Hertfordshire, College Lane, Hatfield AL10 9AB, UK
[42] Max-Planck-Institut für Radioastronomie, Auf dem Hügel 69, 53121 Bonn, Germany
[43] Department of Physics, Center for Cosmology and Astro-Particle Physics, The Ohio State University, Columbus, OH 43210, USA
[44] Department of Physics, Royal Institute of Technology (KTH), AlbaNova, SE-106 91 Stockholm, Sweden
[45] Waseda University, 1-104 Totsukamachi, Shinjuku-ku, Tokyo, 169-8050, Japan
[46] Cosmic Radiation Laboratory, Institute of Physical and Chemical Research (RIKEN), Wako, Saitama 351-0198, Japan
[47] Department of Physics, University of Washington, Seattle, WA 98195-1560, USA
[48] Centre d'Étude Spatiale des Rayonnements, CNRS/UPS, BP 44346, F-30128 Toulouse Cedex 4, France
[49] University College Dublin, Belfield, Dublin 4, Republic of Ireland
[50] Universities Space Research Association (USRA), Columbia, MD 21044, USA
[51] Istituto Nazionale di Fisica Nucleare, Sezione di Roma "Tor Vergata," I-00133 Roma, Italy
[52] Department of Physics and Astronomy, University of Denver, Denver, CO 80208, USA
[53] Institute of Space and Astronautical Science, JAXA, 3-1-1 Yoshinodai, Sagamihara, Kanagawa 229-8510, Japan
[54] Institut für Astro- und Teilchenphysik and Institut für Theoretische Physik, Leopold-Franzens-Universität Innsbruck, A-6020 Innsbruck, Austria
[55] Institut de Ciencies de l'Espai (IEEC-CSIC), Campus UAB, 08193 Barcelona, Spain
[56] Space Sciences Division, NASA Ames Research Center, Moffett Field, CA 94035-1000, USA
[57] NYCB Real-Time Computing Inc., Lattingtown, NY 11560-1025, USA
[58] Department of Chemistry and Physics, Purdue University Calumet, Hammond, IN 46323-2094, USA
[59] Institució Catalana de Recerca i Estudis Avançats (ICREA), Barcelona, Spain
[60] Consorzio Interuniversitario per la Fisica Spaziale (CIFS), I-10133 Torino, Italy
[61] Dipartimento di Fisica, Università di Roma "Tor Vergata," I-00133 Roma, Italy
[62] School of Pure and Applied Natural Sciences, University of Kalmar, SE-391 82 Kalmar, Sweden
Received 2009 September 14; accepted 2009 October 21; published 2009 November 3

ABSTRACT

We report on the observation of the bright, long gamma-ray burst (GRB), GRB 090902B, by the Gamma-ray Burst Monitor (GBM) and Large Area Telescope (LAT) instruments on-board the *Fermi* observatory. This was one of the brightest GRBs to have been observed by the LAT, which detected several hundred photons during the prompt phase. With a redshift of $z = 1.822$, this burst is among the most luminous detected by *Fermi*. Time-resolved spectral analysis reveals a significant power-law component in the LAT data that is distinct from the usual Band model emission that is seen in the sub-MeV energy range. This power-law component appears to extrapolate from the GeV range to the lowest energies and is more intense than the Band component, both below ∼50 keV and above 100 MeV. The Band component undergoes substantial spectral evolution over the entire course of the burst, while the photon index of the power-law component remains constant for most of the prompt phase, then hardens significantly toward the end. After the prompt phase, power-law emission persists in the LAT data as late as 1 ks post-trigger, with its flux declining as $t^{-1.5}$. The LAT detected a photon with the highest energy so far measured from a GRB, $33.4^{+2.7}_{-3.5}$ GeV. This event arrived 82 s after the GBM trigger and ∼50 s after the prompt phase emission had ended in the GBM band. We discuss the implications of these results for models of GRB emission and for constraints on models of the extragalactic background light.

Key words: gamma rays: bursts

1. INTRODUCTION

The *Fermi* Gamma-ray Space Telescope hosts two instruments, the Large Area Telescope (LAT; Atwood et al. 2009) and the Gamma-ray Burst Monitor (GBM; Meegan et al. 2009), which together are capable of measuring the spectral parameters of gamma-ray bursts (GRBs) across seven decades in energy. Since the start of GBM and LAT science operations in early August 2008, emission at energies >100 MeV has been detected from ten GRBs. These detections were made possible by the LAT's greater sensitivity and shorter dead time (26 μs) compared to previous instruments. Prior to *Fermi*, high-energy gamma rays from GRBs with energies up to 18 GeV were observed by the EGRET instrument on-board the *Compton Gamma-ray Observatory*. The EGRET observations suggested three types of high-energy emission: an extrapolation of the low energy spectra to the >100 MeV band (e.g., Dingus et al. 1998), an additional spectral component during the prompt emission (González et al. 2003; Kaneko et al. 2008), and in the case of GRB 940217, a GeV afterglow which was detectable for 90 minutes after the trigger (Hurley et al. 1994). The redshifts of these events were not determined. Recently, Giuliani et al. (2008) reported that GRB 080514B which triggered *AGILE* at lower energies was detected by the Gamma Ray Imaging Detector (GRID) instrument up to 300 MeV. A photometric redshift of $z = 1.8^{+0.4}_{-0.3}$ was reported for this event (Rossi et al. 2008).

In the *Fermi* era, due to the advanced localization capabilities of the LAT and the rapid follow-up by the *Swift* narrow field instruments (Gehrels et al. 2004) and the ground-based

[63] Royal Swedish Academy of Sciences Research Fellow, funded by a grant from the K. A. Wallenberg Foundation.
[64] NASA Postdoctoral Program Fellow, NSSTC, 320 Sparkman Drive, Huntsville, AL 35805, USA.

follow-up community, redshifts for five of the ten LAT bursts have been measured. These include GRB 080916C with $z = 4.35 \pm 0.15$ (Greiner et al. 2009), a long burst that has the highest inferred isotropic energy, $E_{\rm iso} \approx 8.8 \times 10^{54}$ erg (10 keV–10 GeV; Abdo et al. 2009c), and GRB 090510 with $z = 0.903 \pm 0.003$ (Rau et al. 2009), the second short burst seen by the LAT and the first short burst to show definitively an additional hard power-law component in the GeV band during the prompt phase (Abdo et al. 2009a).

GRB 090902B is a long, fairly intense burst with a redshift of $z = 1.822$ (Cucchiara et al. 2009) and a fluence of $(4.36 \pm 0.06) \times 10^{-4}$ erg cm^{-2} (10 keV–10 GeV) over the first 25 s of the prompt emission. These data give an isotropic energy $E_{\rm iso} = (3.63 \pm 0.05) \times 10^{54}$ erg, comparable to that of GRB 080916C. Similar to GRB 090510, GRB 090902B has a significant additional, hard power-law component that appears during the prompt phase. Furthermore, a spectral feature at energies $\lesssim$50 keV is evident in the GBM spectrum of GRB 090902B that is consistent with an extrapolation of the >100 MeV power-law emission down to those energies. In previous analyses, Preece et al. (1996) reported evidence for an additional low-energy spectral component below 20 keV for ~15% of BATSE bursts.

We report on the observations and analysis of gamma-ray emission from GRB 090902B measured by the GBM and LAT instruments. In Section 2, we present details of the detections by both instruments and summarize the follow-up observations. In Section 3, we show the light curves of the prompt emission as seen by the various detectors and describe the extended emission found in the LAT data out to 1 ks after the trigger. In Section 4, we present the time-resolved spectral analysis of the burst emission during the prompt phase. Finally, in Section 5, we discuss the physical interpretation of the GBM and LAT data, focusing on the implications of the power-law component for models of GRB physics.

2. OBSERVATIONS

On 2009 September 2 at 11:05:08.31 UT, the *Fermi* GBM triggered on and localized the bright burst GRB 090202B (trigger 273582310/090902462, Bissaldi & Connaughton 2009). The burst was within the LAT field-of-view (FOV) initially at an angle of 51° from the boresight. This event was sufficiently bright in the GBM that an Autonomous Repoint Request was made, and the spacecraft began slewing within 10 s toward the burst. After ~200 s, it had pointed the LAT boresight to within a few degrees of the final burst localization. It maintained that pointing until ~1 ks post-trigger, when the Earth's limb began to enter the LAT FOV. This burst was detected up to ~5 MeV by GBM, and emission was significantly detected by the LAT, with 39 photons above 1 GeV. The highest energy photon had $E = 33.4^{+2.7}_{-3.5}$ GeV and arrived 82 s after the GBM trigger; and the initial analyses detected photons as late as 300 s after the trigger (de Palma et al. 2009).

From the LAT data, the burst was localized to R.A. (J2000), decl. (J2000) = 265.00, 27.33 with a statistical uncertainty of 0.°04 (+ < 0.°1 systematic), enabling Target of Opportunity (ToO) observations to begin ~12.5 hr after the trigger with the narrow field instruments on *Swift*. A candidate X-ray afterglow within the LAT error circle was detected by the X-Ray Telescope (XRT; Kennea & Stratta 2009). This source was confirmed to be fading (Stratta et al. 2009), and UltraViolet and Optical Telescope (UVOT) observations revealed the optical afterglow (Swenson & Stratta 2009). The earliest ground-based optical observations were obtained by ROTSE-IIIa ~1.4 hr post-trigger (Pandey et al. 2009). Other detections were reported in the optical (Perley et al. 2009), in the near infrared by GROND (Olivares et al. 2009), and in the radio (van der Horst et al. 2009; Chandra & Frail 2009). The location of the fading source detected by GROND was R.A. (J2000), decl.(J2000) = $17^{\rm h}39^{\rm m}45\overset{\rm s}{.}41$, $+27^\circ19'27\overset{''}{.}1$, 3.3 arcmin from the LAT location (Olivares et al. 2009). The afterglow redshift of $z = 1.822$ was measured by Cucchiara et al. (2009) using the GMOS spectrograph mounted on the Gemini–North telescope.

3. LIGHT CURVES

In Figure 1, we show the GBM and LAT light curves in several energy bands. The top three panels show data from the most brightly illuminated Na I and BGO detectors of the GBM, and the bottom three panels show the LAT data with various event selections. In the bottom panel, the measured photon energies are plotted as a function of time, including the highest energy event ($E = 33.4$ GeV) that arrived 82 s after the GBM trigger time, T_0. From the GBM light curves, we see that at energies $\lesssim$1 MeV, the prompt phase ends approximately 25 s after T_0. Detailed analysis of the GBM data for energies 50–300 keV yields a formal T90 duration[65] of 21.9 s starting at $T_0 + 2.2$ s. By contrast, the LAT emission >100 MeV clearly continues well after this time range.

On timescales longer than the prompt phase, the LAT detects emission from GRB 090902B as late as 1 ks after the GBM trigger. The spectrum of this emission is consistent with a power law with photon index $\Gamma = -2.1 \pm 0.1$, and its flux (>100 MeV) declines as $t^{-1.5\pm0.1}$ over the interval (T_0+25, T_0+1000 s). As we note above, the LAT observations are interrupted by entry of the Earth's limb into the FOV, but analysis of data after $T_0 + 3600$ s, when the source location is again unocculted, shows that any later emission lies below the LAT sensitivity (Figure 2). The upper limit we obtain for data after $T_0 + 3600$ is consistent with an extrapolation of the $t^{-1.5}$ decay. Similar late time emission for energies >100 MeV that extends well beyond the prompt phase has been seen for five earlier bursts by *Fermi*: GRB 080916C (Abdo et al. 2009c), GRB 090323 (Ohno et al. 2009), GRB 090328 (Cutini et al. 2009), GRB 090510, independently seen by *AGILE* (Giuliani et al. 2009) and by *Fermi* (Ghirlanda et al. 2009), and GRB 090626 (Piron et al. 2009).

4. TIME-RESOLVED SPECTRAL ANALYSIS

Spectral analysis was performed using the data from both the GBM and the LAT. These analyses include data from the Na I detectors 0, 1, 2, 9, 10 and BGO detectors, and LAT "transient" class data, with front- and back-converting events considered separately. The Na I data are fitted from 8 keV to 1 MeV and the BGO from 250 keV to 40 MeV using the Time Tagged Event (TTE) data, which are high time resolution data that allow us to define the time intervals based on the structure of the GBM and LAT light curves. The LAT data are fitted from 100 MeV to 200 GeV. An effective area correction of 0.9 has been fitted to the BGO data to match the model normalizations given by the Na I data; this correction is consistent with the uncertainties in the GBM detector responses. The fits were performed with the spectral analysis software package RMFIT (version 3.1). For further details on the data extraction and spectral analysis procedures, see Abdo et al. (2009b) and A. A. Abdo et al. (2009, in preparation).

[65] The T90 duration is the time over which the central 90% of the counts from the burst have been accumulated.

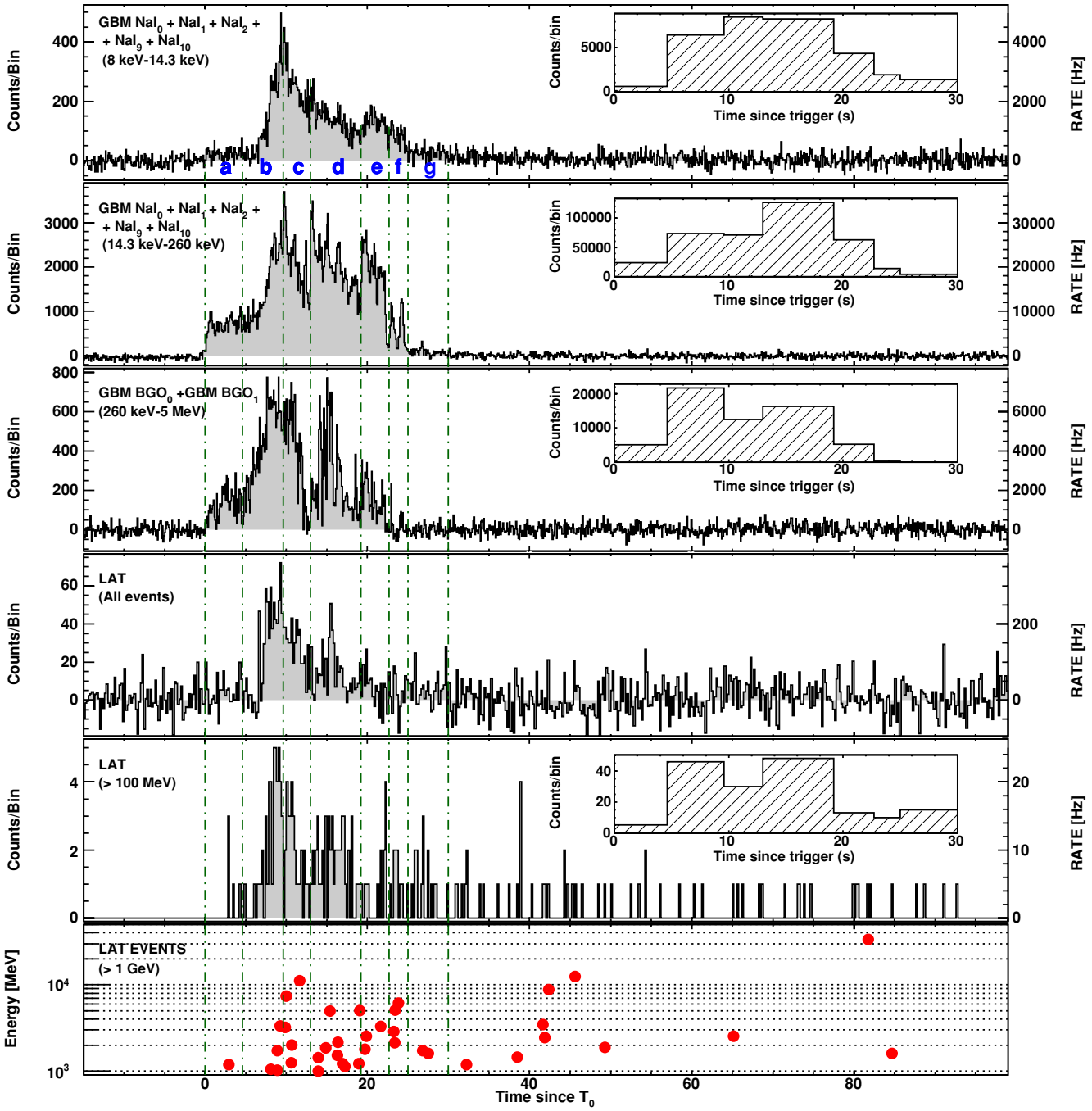

Figure 1. GBM and LAT light curves for the gamma-ray emission of GRB 090902B. The data from the GBM NaI detectors were divided into soft (8–14.3 keV) and hard (14.3–260 keV) bands in order to reveal any obvious similarities between the light curve at the lowest energies and that of the LAT data. The fourth panel shows all LAT events that pass the on-board gamma filter, while the fifth and sixth panels show data for the "transient" class event selection for energies >100 MeV and >1 GeV, respectively. The vertical lines indicate the boundaries of the intervals used for the time-resolved spectral analysis. Those time boundaries are at T_0 + (0, 4.6, 9.6, 13.0, 19.2, 22.7, 25.0, 30.0) s. The insets show the counts for the corresponding data set binned using these intervals in order to illustrate the relative numbers of counts considered in each spectral fit.

The time-integrated spectrum of GRB 090902B is best modeled by a Band function (Band et al. 1993) and a power-law component (Table 1). The power-law component significantly improves the fit between 8 keV and 200 GeV both in the time-integrated spectrum and in the individual time intervals where there are sufficient statistics. It is also required when considering only the GBM data (8 keV–40 MeV) for the time-integrated spectrum, as its inclusion causes an improvement of ≈ 2000 in the CSTAT statistic over the Band function alone. When data below $\sim$50 keV are excluded, a power-law component can be neglected in the GBM-only fits. We conclude that this power-law component contributes a significant part of the emission both at low (<50 keV) and high (>100 MeV) energies. Figure 3 shows the counts and unfolded νF_ν spectra for a Band function with a power-law component fitted to the data for interval **b** (when the low energy excess is most significant) using the parameters given in Table 1.

Spectral evolution is apparent in the Band function component from the changing $E_{\rm peak}$ values throughout the burst, while β remains soft until interval **e** when it hardens significantly. β

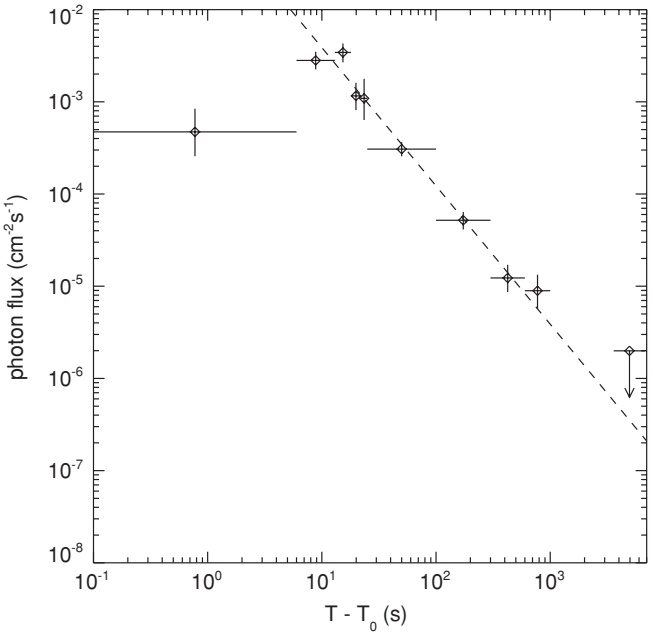

Figure 2. Light curve of GRB 090902B for energies 0.1–300 GeV from unbinned likelihood fits to the LAT data. After the prompt phase, extended or afterglow emission consistent with a temporal profile $\propto t^{-1.5}$ (dashed line) lasts until $\sim T_0 + 1000$ s. The upper limit at times $> T_0 + 3600$ s was derived from the data collected after the source emerged from occultation by the Earth.

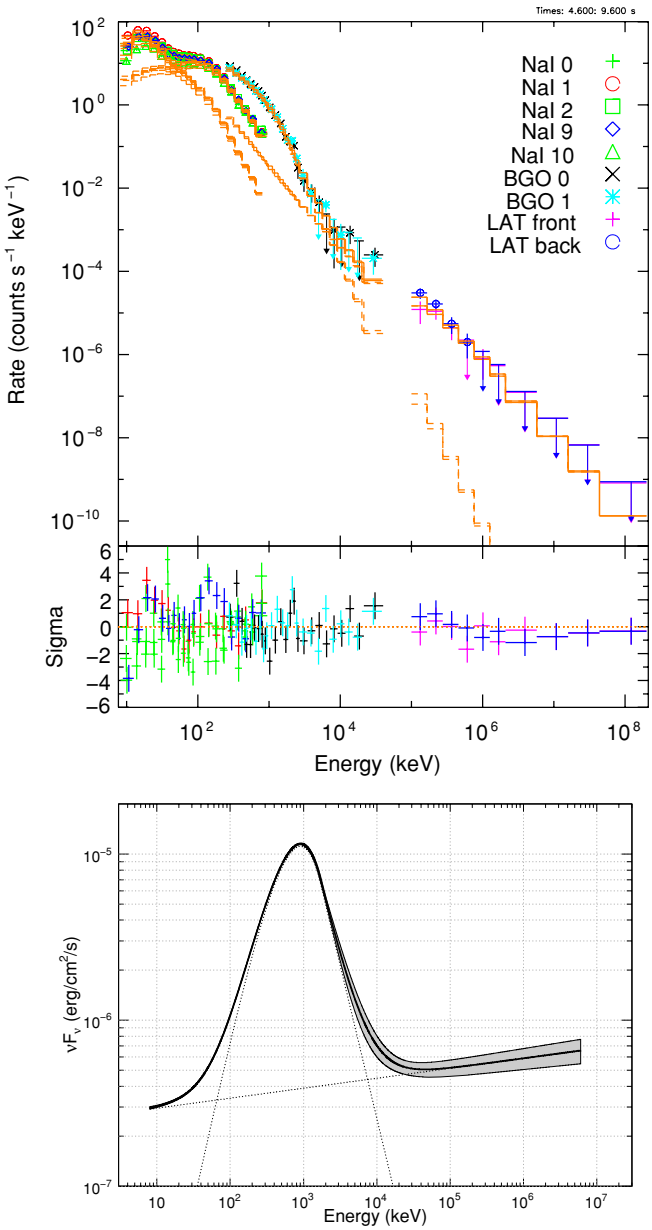

Figure 3. Joint fit of GBM and LAT data to interval **b**, (T_0+4.6, T_0+9.6 s). Top: counts spectrum; separate model components are plotted, Band (dashed), power law (solid). Bottom: unfolded νF_ν spectrum. The extension of the >100 MeV power-law component to the lowest energies (<50 keV) is shown.

is similarly hard in interval **f**, after which the Band function component is no longer detected. The hardening of β is accompanied by an apparent hardening of the power-law index, Γ, which until interval **e** does not exhibit much variation. However, this is not definitive since the flux is too low to constrain Γ in intervals **e** and **f** separately. A spectral fit of the sum of these two intervals confirms the presence of both a harder β and a harder Γ, with a clear statistical preference for the inclusion of the power-law component. An equally good fit is obtained in the combined **e** + **f** interval if this power law has an exponential cutoff at high energies, with the preferred cutoff energy lying above 2 GeV. Finally, we note that in interval **b**, a marginally better fit is achieved using a model with the additional power-law component having an exponential cutoff at high energies. The improvement is at the $\sim 3\sigma$ level and indicates weak evidence for a cutoff in the second component, placing a lower limit on the cutoff energy in this interval of about 1 GeV.

5. DISCUSSION AND INTERPRETATION

The *Fermi* data for GRB 090902B show for the first time clear evidence of excess emission both at low energies ($\lesssim$ 50 keV) and at high energies (>100 MeV), while the Band function alone fits data at intermediate energies adequately. These excesses are well fitted by a single power-law component suggesting a common origin. This power-law component accounts for ≈24% of the total fluence in the 10 keV–10 GeV range, and its photon index is hard, with a value ~ -1.9 throughout most of the prompt phase. Such a hard component producing the observed excess at low energies is difficult to explain in the context of leptonic models by the usual synchrotron self-Compton (SSC) mechanisms. In the simplest versions of these models, the peak of the SSC emission is expected to have a much higher energy than the synchrotron peak at MeV energies, and the SSC component has a soft tail that is well below the synchrotron flux at lower energies and so would not produce excess emission below ∼50 keV. Hadronic models, either in the form of proton synchrotron radiation (Razzaque et al. 2009) or photohadronic interactions (Asano et al. 2009), can produce a hard component with a similar low energy excess via direct and cascade radiation (e.g., synchrotron emission by secondary pairs at low energies). However, the total energy release in hadronic models would exceed the observed gamma-ray energy of $E_{\rm iso} = 3.63 \times 10^{54}$ erg significantly and may pose a challenge for the total energy budget. Collimation into a narrow jet may alleviate the energy requirements, since the actual energy release from GRB 090902B can be smaller by a jet beaming factor $> 1/\Gamma_0^2$ from the apparent isotropic value, where Γ_0 is the bulk Lorentz factor of the fireball.

From the observation of a $11.16^{+1.48}_{-0.58}$ GeV photon in interval **c**, the highest energy during the prompt phase and thus the most constraining, we derive a minimum value of the bulk

Table 1
Band function + Power-Law Fit Parameters for the Time-Resolved Spectral Fits

Interval	Time Range (s)	$E_{\rm peak}$ (kev)	α	β	Γ	CSTAT/DOF	ΔCSTAT	Energy Fluence (erg cm^{-2}, 8 keV–30 GeV)
...	0.0–30.0	726 ($\pm$8)	-0.61 ($\pm$0.01)	-3.8 ($^{+0.2}_{-0.3}$)	-1.93($^{+0.01}_{-0.01}$)	2562/963	2005	(4.59 $\pm$ 0.05) $\times10^{-4}$
a	0.0–4.6	526 ($\pm$12)	-0.09 ($\pm$0.04)	-3.7 ($^{+0.3}_{-0.6}$)	-1.87($^{+0.04}_{-0.05}$)	901/963	43	(3.72 $\pm$ 0.13) $\times10^{-5}$
b	4.6– 9.6	908 ($^{+15}_{-14}$)	0.07 ($\pm$0.03)	-3.9 ($^{+0.2}_{-0.3}$)	-1.94 ($\pm$0.02)	1250/963	3165	(1.44 $\pm$ 0.03) $\times10^{-4}$
c	9.6–13.0	821 ($\pm$16)	-0.26 ($\pm$0.03)	-5.0($^{+0.8}_{-\infty}$)	-1.98 ($\pm$0.02)	1310/963	2109	(9.42 $\pm$ 0.24) $\times10^{-5}$
d	13.0–19.2	529 ($\pm$9)	-0.65 (±-0.02)	-3.2 ($^{+0.1}_{-0.2}$)	-1.86 ($\pm$ 0.02)	1418/963	199	(1.29 $\pm$0.03) $\times10^{-4}$
e	19.2–22.7	317 ($\pm$8)	-0.78 (±-0.02)	-2.4 ($\pm$0.1)	...	1117/965	...	(4.8 $\pm$ 0.2) $\times10^{-5}$
f	22.7–25.0	236 ($^{+25}_{-33}$)	-1.30 ($^{+0.04}_{-0.03}$)	-2.2 ($\pm$0.1)	...	1077/965	...	(1.0 $\pm$ 0.1) $\times10^{-5}$
e+f	19.2–25.0	327 ($\pm$8)	-0.91 ($\pm$0.02)	-2.6 ($\pm$0.1)	-1.59 ($\pm$0.20)	1219/963	16	(6.1 $\pm$0.4) $\times10^{-5}$
g	25.0–30.0	...	...	...	-1.93 ($^{+0.25}_{-0.26}$)	1209/967	...	(6.8 $\pm$ 0.8) $\times10^{-6}$

Notes. The time range values are relative to the trigger time T_0. The column ΔCSTAT gives the change in CSTAT when fitting with only the Band function versus Band+power law. The Band function is given by

$$n(E) = A\left(\frac{E}{100\ \text{keV}}\right)^{\alpha}\exp\left(-\frac{E(2+\alpha)}{E_{\rm peak}}\right), \qquad E < E_c,$$
$$= A\left(\frac{(\alpha-\beta)E_{\rm peak}}{100\ \text{keV}(2+\alpha)}\right)^{\alpha-\beta}\exp(\beta-\alpha)\left(-\frac{E}{100\ \text{keV}}\right)^{\beta}, \quad E \geqslant E_c, \tag{1}$$

where $E_c = (\alpha-\beta)E_{\rm peak}/(2+\alpha)$ (Band et al. 1993). The power-law function is given by

$$n(E) = A\left(\frac{E}{100\ \text{keV}}\right)^{\Gamma}. \tag{2}$$

Lorentz factor $\Gamma_{\rm min} \approx 1000$ using the flux variability timescale of $t_v \approx 53$ ms found in the BGO data. This limit follows from the constraint that the opacity for $e^{\pm}$ pair production with target photons fitted by the Band+PL model in interval **c** is less than unity for the 11.16 GeV photon (see, e.g., Fenimore et al. 1993; Baring & Harding 1997; Lithwick & Sari 2001). This high $\Gamma_{\rm min}$ value is of the same order as the values derived for GRB 080916C (Abdo et al. 2009c) and GRB 090510 (Abdo et al. 2009a), both of which have been detected at >10 GeV with the LAT.

The delayed onset of the $\gtrsim$100 MeV emission from the GBM trigger has been modeled for GRB 080916C as arising from proton synchrotron radiation in the prompt phase (Razzaque et al. 2009) and for GRB 090510 as arising from electron synchrotron radiation in the early afterglow phase (Kumar & Barniol Duran 2009; Ghirlanda et al. 2009). In order to produce the peak of the LAT emission at $\sim T_0 + 9$ s in the early afterglow scenario for GRB 090902B from deceleration of the GRB fireball, a value of $\Gamma_0 \approx 1000$ is required. This is similar to $\Gamma_{\rm min}$ that we calculate, but the observed large amplitude variability on short timescales ($\approx$90 ms) in the LAT data, which is usually attributed to prompt emission, argues against such models. Also, the appearance of the power-law component extending down to $\approx$8 keV within only a few seconds of the GRB trigger disfavors an afterglow interpretation. The proton synchrotron model, on the other hand, requires a rather large total energy budget, as mentioned previously.

Yet another interpretation of the observed excess in the high and low energies may be provided by two non-thermal power-law components along with a thermal component from the jet photosphere (Mészáros & Rees 2000; Ryde 2004). The thermal component, broadened by temperature variations, then accounts for the $\gtrsim$100 keV–few MeV emission with $\Gamma_0 \approx 930$ (Pe'er et al. 2007), although fits of such a model to our data do not improve over the Band+PL model. Furthermore, it is difficult for the photospheric model to explain the delayed onset of the $\gtrsim$100 MeV emission.

The detection of the 33.4 GeV photon, 82 s after the GRB trigger and well after the soft gamma-ray emission subsided, may help constrain the origin of the late-time decay of the power-law component, which goes as $t^{-1.5}$. A synchrotron origin of the 33.4 GeV photon would be difficult since it would require significant energy gain by electrons over a gyroradius and a bulk Lorentz factor >1500. In the case of diffusive shock acceleration, the energy losses in the upstream region of the shock may dominate (see, e.g., Li & Waxman 2006) and prevent acceleration of electrons to an energy high enough to radiate a 33.4 GeV photon. An interpretation by afterglow SSC emission is still possible, however.

The constraints on the quantum gravity mass scale from GRB 090902B using the time of flight test (Amelino-Camelia et al. 1998) are much weaker than those from GRB 090510 (Abdo et al. 2009a) due to the larger interval, 82 s, between T_0 and the arrival time of the 33.4 GeV photon. However, the moderately high redshift ($z = 1.822$) of GRB 090902B allows us to use this photon to probe and constrain models of the extragalactic background light (EBL; Kneiske et al. 2004; Metcalfe et al. 2003; Stecker et al. 2006; Franceschini et al. 2008; Gilmore et al. 2009; Finke et al. 2009). The 33.4 GeV photon would not be absorbed by the EBL in any models except for the "fast evolution" and the "baseline" models by Stecker et al. (2006), which give optical depths of $\tau_{\gamma\gamma} = 7.7$ and 5.8, respectively. We have performed spectral fits of the LAT data with and without the predicted EBL absorption from Stecker's models assuming a simple power law as the intrinsic emission model. Based on Monte Carlo simulations, we found that Stecker's fast evolution and baseline models are disfavored at a $>3\sigma$ level.

In summary, GRB 090902B is one of the brightest bursts detected by the GBM and LAT instruments on *Fermi*. It

clearly shows excess emission at high and low energies during the prompt phase, requiring a hard power-law component in addition to the usual Band function in order to fit the data. The origin of this component is not understood, and its presence in this burst poses genuine challenges for the theoretical models. Like the other two bright *Fermi* bursts detected by the LAT, GRB 080916C and GRB 090510, GRB 090902B appears to possess a very high Lorentz factor for the bulk outflow, $\Gamma \approx 1000$, and has some suggestion of a delayed onset of the emission above $\sim$100 MeV. Finally, the 33.4 GeV photon, the highest energy yet detected from a GRB, and the $z = 1.822$ redshift of this burst have allowed us to place significant constraints on some models of the EBL.

The *Fermi* LAT Collaboration acknowledges support from a number of agencies and institutes for both development and the operation of the LAT as well as scientific data analysis. These include NASA and DOE in the United States, CEA/Irfu and IN2P3/CNRS in France, ASI and INFN in Italy, MEXT, KEK, and JAXA in Japan, and the K. A. Wallenberg Foundation, the Swedish Research Council and the National Space Board in Sweden. Additional support from INAF in Italy and CNES in France for science analysis during the operations phase is also gratefully acknowledged.

REFERENCES

Abdo, A. A., et al. 2009a, Nature, in press
Abdo, A. A., et al. 2009b, ApJ, in press
Abdo, A. A., et al. 2009c, Science, 323, 1688
Amelino-Camelia, G., Ellis, J., Mavromatos, N. E., Nanopoulos, D. V., & Sarkar, S. 1998, Nature, 395, 525
Asano, K., Guiriec, S., & Mészáros, P. 2009, ApJ, 705, L191
Atwood, W. B., et al. 2009, ApJ, 697, 1071
Band, D., et al. 1993, ApJ, 413, 281
Baring, M. G., & Harding, A. K. 1997, ApJ, 491, 663
Bissaldi, E., & Connaughton, V. 2009, GRB Coordinates Network, 9866, 1
Chandra, P., & Frail, D. A. 2009, GRB Coordinates Network, 9889, 1
Cucchiara, A., Fox, D. B., Tanvir, N., & Berger, E. 2009, GRB Coordinates Network, 9873, 1
Cutini, S., Vasileiou, V., & Chiang, J. 2009, GRB Coordinates Network, 9077, 1
de Palma, F., Bregeon, J., & Tajima, H. 2009, GRB Coordinates Network, 9867, 1
Dingus, B. L., Catelli, J. R., & Schneid, E. J. 1998, in AIP Conf. Ser. 428, Gamma-Ray Bursts, 4th Hunstville Symposium, ed. C. A. Meegan, R. D. Preece, & T. M. Koshut (New York: AIP), 349
Fenimore, E. E., Epstein, R. I., & Ho, C. 1993, A&AS, 97, 59
Finke, J. D., Razzaque, S., & Dermer, C. D. 2009, arXiv:0905.1115
Franceschini, A., Rodighiero, G., & Vaccari, M. 2008, A&A, 487, 837
Gehrels, N., et al. 2004, ApJ, 611, 1005
Ghirlanda, G., Ghisellini, G., & Nava, L. 2009, arXiv:0909.0016
Gilmore, R. C., Madau, P., Primack, J. R., Somerville, R. S., & Haardt, F. 2009, MNRAS, in press (arXiv:0905.1144)
Giuliani, A., et al. 2008, A&A, 491, L25
Giuliani, A., et al. 2009, ApJL, in press
González, M. M., Dingus, B. L., Kaneko, Y., Preece, R. D., Dermer, C. D., & Briggs, M. S. 2003, Nature, 424, 749
Greiner, J., et al. 2009, A&A, 498, 89
Hurley, K., et al. 1994, Nature, 372, 652
Kaneko, Y., González, M. M., Preece, R. D., Dingus, B. L., & Briggs, M. S. 2008, ApJ, 677, 1168
Kennea, J., & Stratta, G. 2009, GRB Coordinates Network, 9868
Kneiske, T. M., Bretz, T., Mannheim, K., & Hartmann, D. H. 2004, A&A, 413, 807
Kumar, P., & Barniol Duran, R. 2009, MNRAS, in press (arXiv:0905.2417)
Li, Z., & Waxman, E. 2006, ApJ, 651, 328
Lithwick, Y., & Sari, R. 2001, ApJ, 555, 540
Meegan, C., et al. 2009, ApJ, 702, 791
Mészáros, P., & Rees, M. J. 2000, ApJ, 530, 292
Metcalfe, L., et al. 2003, A&A, 407, 791
Ohno, M., Cutini, S., McEnery, J., Chiang, J., & Koerding, E. 2009, GRB Coordinates Network, 9021, 1
Olivares, F., Afonso, F., Greiner, J., McBreen, S., Kruehler, T., Rau, A., Yoldas, A., & G., K. 2009, GRB Coordinates Network, 9874, 1
Pandey, S. B., Zheng, W., Yuan, F., & Akerlof, C. 2009, GRB Coordinates Network, 9878, 1
Pe'er, A., Ryde, F., Wijers, R. A. M. J., Mészáros, P., & Rees, M. J. 2007, ApJ, 664, L1
Perley, D., Kleiser, I. K. W., & Rex, J. M. 2009, GRB Coordinates Network, 9870, 1
Piron, F., Longo, F., Iafrate, G., Cheung, T., Tajima, H., & Connaughton, V. 2009, GRB Coordinates Network, 9584, 1
Preece, R. D., Briggs, M. S., Pendleton, G. N., Paciesas, W. S., Matteson, J. L., Band, D. L., Skelton, R. T., & Meegan, C. A. 1996, ApJ, 473, 310
Rau, A., McBreen, S., Kruehler, T., & Greiner, J. 2009, GRB Coordinates Network, 9353, 1
Razzaque, S., Dermer, C. D., & Finke, J. D. 2009, arXiv:0908.0513
Rossi, A., et al. 2008, A&A, 491, L29
Ryde, F. 2004, ApJ, 614, 827
Stecker, F. W., Malkan, M. A., & Scully, S. T. 2006, ApJ, 648, 774
Stratta, G., D'Elia, V., & Perri, M. 2009, GRB Coordinates Network, 9876, 1
Swenson, C. A., & Stratta, G. 2009, GRB Coordinates Network, 9877, 1
van der Horst, A. J., Kamble, A. P., Wijers, R. A. M. J., & Kouveliotou, C. 2009, GRB Coordinates Network, 9883, 1